Aberrant early endosome biogenesis mediates complement activation in the retinal pigment epithelium in models of macular degeneration

Gulpreet Kaur[a,b,c,1], Li Xuan Tan[a,b,d,1,2], Gurugirijha Rathnasamy[a,b,2], Nilsa La Cunza[a,b,d,2], Colin J. Germer[a,b,d,2], Kimberly A. Toops[a,b], Marie Fernandes[e], Timothy A. Blenkinsop[e], and Aparna Lakkaraju[a,b,c,d,2,3]

[a]Department of Ophthalmology and Visual Sciences, School of Medicine and Public Health, University of Wisconsin–Madison, Madison, WI 53706; [b]McPherson Eye Research Institute, University of Wisconsin–Madison, Madison, WI 53706; [c]Cellular and Molecular Biology Graduate Program, University of Wisconsin–Madison, Madison, WI 53706; [d]Division of Pharmaceutical Sciences, School of Pharmacy, University of Wisconsin–Madison, Madison, WI 53706; and [e]Cell, Developmental & Regenerative Biology, Icahn School of Medicine at Mount Sinai, New York, NY 10029

Edited by Catherine Bowes Rickman, Duke University Medical Center, Durham, NC, and accepted by Editorial Board Member Jeremy Nathans July 26, 2018 (received for review March 22, 2018)

Abnormally enlarged early endosomes (EEs) are pathological features of neurodegenerative diseases, yet insight into the mechanisms and consequences of EE expansion remains elusive. Here, we report swollen apical EEs in the retinal pigment epithelium (RPE) of aged human donors and in the pigmented *Abca4*$^{-/-}$ mouse model of Stargardt early-onset macular degeneration. Using high-resolution live-cell imaging, we show that age-related and pathological accumulation of lipofuscin bisretinoids increases ceramide at the apical surface of the RPE, which promotes inward budding and homotypic fusion of EEs. These enlarged endosomes internalize the complement protein C3 into the RPE, resulting in the intracellular generation of C3a fragments. Increased C3a in turn activates the mechanistic target of rapamycin (mTOR), a regulator of critical metabolic processes such as autophagy. The antidepressant desipramine, which decreases ceramide levels by inhibiting acid sphingomyelinase, corrects EE defects in the RPE of *Abca4*$^{-/-}$ mice. This prevents C3 internalization and limits the formation of C3a fragments within the RPE. Although uncontrolled complement activation is associated with macular degenerations, how complement contributes to pathology in a progressive disease is not well understood. Our studies link expansion of the EE compartment with intracellular complement generation and aberrant mTOR activation, which could set the stage for chronic metabolic reprogramming in the RPE as a prelude to disease. The pivotal role of ceramide in driving EE biogenesis and fusion in the *Abca4*$^{-/-}$ mice RPE suggests that therapeutic targeting of ceramide could be effective in Stargardt disease and other macular degenerations.

Ceramide | endosome biogenesis | intracellular complement activation | clinically approved drugs | macular degeneration

Cell fate decisions in eukaryotes are regulated by an elaborate and dynamic network of organelles that communicate with one another and with the extracellular environment to maintain tissue homeostasis (1). Key players in this network are early endosomes (EEs), primary hubs that sort internalized cargo and modulate diverse processes, such as signaling, metabolism, and inflammation (2, 3). Abnormally enlarged EEs and subsequent endolysosomal dysfunction are early signs of neurodegenerative diseases, including Alzheimer's disease (AD) and Niemann–Pick type C disease. Endosomal defects in these diseases manifest before other deficits, suggesting that they could drive downstream pathology (4). Specific mechanisms that cause EE expansion, and how this contributes to disease, are not well understood.

In the retina, efficient endolysosome function in the retinal pigment epithelium (RPE) is essential for clearing phagocytosed photoreceptor outer segments (OS) and disposing cellular debris by autophagy, which helps maintain RPE and photoreceptor health (5). Intriguingly, recent studies suggest a novel role for endosomes—specifically EEs—in modulating complement-mediated inflammation (2). This is pertinent for the RPE because aberrant complement activity and increased inflammation are associated with Stargardt inherited macular dystrophy and age-related macular degeneration (AMD), which cause central vision loss in over 30 million people worldwide (6, 7). Little is currently known regarding mechanisms that regulate the formation and function of EEs in the RPE, and how these organelles can participate in driving pathology.

In the pigmented *Abca4*$^{-/-}$ mouse model of Stargardt disease, we have reported that accelerated formation of lipofuscin bisretinoids in the RPE leads to cholesterol accumulation, which activates acid sphingomyelinase (ASMase), the enzyme that hydrolyzes sphingomyelin to ceramide. Increased ceramide derails organelle traffic by stabilizing microtubules (8), and prevents endosomal recycling of complement regulatory proteins and lysosome-mediated membrane repair after complement attack (9).

Significance

The first lines of communication between cells and the environment are early endosomes, which sort incoming cargo to regulate cell health. Endosomal abnormalities are seen in neurodegenerative diseases, yet the molecular mechanisms remain obscure. Here, using human donor cells and disease models, we demonstrate that excess ceramide promotes expansion of early endosomes in the retinal pigment epithelium (RPE), a primary site of injury in Stargardt and age-related maculopathies. Complement C3 uptake into enlarged endosomes and subsequent cleavage is associated with abnormal mechanistic target of rapamycin activity. Decreasing ceramide using Food and Drug Administration-approved drugs corrects endosomal defects and prevents C3 activation. Our studies establish how organelles modulate RPE complement activity, and identify ceramide as a drug target for macular degenerations.

Author contributions: G.K., L.X.T., G.R., N.L.C., K.A.T., and A.L. designed research; G.K., L.X.T., G.R., N.L.C., C.J.G., K.A.T., and A.L. performed research; M.F. and T.A.B. contributed new reagents/analytic tools; G.K., L.X.T., G.R., N.L.C., K.A.T., and A.L. analyzed data; and G.K., L.X.T., G.R., and A.L. wrote the paper.

The authors declare no conflict of interest.

This article is a PNAS Direct Submission. C.B.R. is a guest editor invited by the Editorial Board.

Published under the PNAS license.

[1]G.K. and L.X.T. contributed equally to this work.

[2]Present address: Department of Ophthalmology, University of California, San Francisco, CA 94143.

[3]To whom correspondence should be addressed. Email: aparna.lakkaraju@ucsf.edu.

This article contains supporting information online at www.pnas.org/lookup/suppl/doi:10.1073/pnas.1805039115/-/DCSupplemental.

Published online August 20, 2018.

Downloaded at Palestinian Territory, occupied on November 26, 2021

www.manaraa.com

Here, using polarized primary human and porcine RPE cultures and *Abca4*$^{-/-}$ mice, we uncover another consequence of increased ceramide on RPE membrane dynamics: accelerated inward budding of EEs from the apical membrane and homotypic fusion of newborn EEs. These enlarged EEs act as conduits for the entry of the complement component C3 into the RPE, resulting in the generation of C3a fragments and activation of mechanistic target of rapamycin (mTOR) (10). The Food and Drug Administration-approved tricyclic antidepressant desipramine, which decreases RPE ceramide by inhibiting ASMase (8, 9), restores EE morphology, prevents intracellular C3a formation, and limits mTOR activation in the RPE of *Abca4*$^{-/-}$ mice. These data connect EE defects with complement activation in the RPE and suggest that repurposing existing drugs known to inhibit ASMase could be a therapeutic strategy for Stargardt disease and other macular degenerations associated with bisretinoid accumulation.

Results

EEs Are Enlarged in RPE from Aged Human Donors and *Abca4*$^{-/-}$ Mice. EEs are characterized by the presence of the small GTPase Rab5, its effector early endosome autoantigen 1 (EEA1), and phosphatidylinositol 3-phosphate [PI(3)P], which confer organelle identity and regulate EE fusion, motility, and function (1). To identify endosomal alterations in aging or diseased RPE, we first examined EE morphology in cultures of aged human RPE by immunostaining for EEA1. Analysis of EE volumes revealed a significant increase in the number of intermediate (1–2 μm^3) and large (>2 μm^3) EEs in aged (60- to 90-y-old) human RPE cultures compared with fetal cultures (Fig. 1*A* and *SI Appendix*, Fig. S1*A*). Because a key difference between fetal and aged human RPE is the age-dependent accumulation of autofluorescent lipofuscin bisretinoids (*SI Appendix*, Fig. S1*B*), we asked if EE expansion tracked with bisretinoid levels. We compared EEA1-labeled organelles in RPE flatmounts from 6-mo-old wild-type mice with those from *Abca4*$^{-/-}$ mice, which are characterized by accelerated bisretinoid accumulation (*SI Appendix*, Fig. S1*C*). As with aged human RPE, we observed an ∼twofold increase in large EEs in *Abca4*$^{-/-}$ RPE compared with wild-type RPE (Fig. 1*B* and *SI Appendix*, Fig. S1*D*). To confirm that bisretinoids were indeed responsible for enlarged EEs, we loaded primary cultures of polarized porcine RPE (11) with A2E at levels comparable to those found in aged human and *Abca4*$^{-/-}$ mice RPE (8), and observed a similar increase in EE volume and numbers in RPE with A2E compared with untreated cells (Fig. 1*C* and *SI Appendix*, Fig. S1*E*).

Bisretinoid-Induced Cholesterol Accumulation Drives EE Expansion in the RPE. High levels of bisretinoids in Stargardt and Best macular dystrophies cause a secondary accumulation of cholesterol in RPE lysosomes (8, 12). Because cholesterol has been implicated in EE expansion in AD (4), we asked if it is also involved in EE expansion in RPE with bisretinoids. We treated aged human RPE (Fig. 2*A* and *SI Appendix*, Fig. S2*A*), *Abca4*$^{-/-}$ mice (Fig. 2*B* and *SI Appendix*, Fig. S2*B*), and A2E-containing primary porcine RPE cultures (Fig. 2*C* and *SI Appendix*, Fig. S2*C*) with TO901317, a liver X receptor (LXR) agonist that increases cholesterol efflux from the RPE by transcriptionally activating cholesterol transporters, such as ABCA1 (8, 9, 13). In all three models, cholesterol removal decreased EE volumes (Fig. 2) and numbers (*SI Appendix*, Fig. S2) in RPE with bisretinoids. Taken together, these data strongly suggest that enlarged EEs in RPE with bisretinoids are a result of excess lysosomal cholesterol in these cells.

Photoreceptor OS Clearance Is Unaffected in RPE with Enlarged EEs. EEs are highly dynamic organelles that undergo continuous membrane remodeling (e.g., tubulation, fission, and fusion), and coordinated maturation of EEs into late endosomes and lysosomes is essential for cargo degradation (1). To explain the increase in EE numbers and volumes seen in RPE with bisretinoids, we investigated three potential mechanisms that could impact EE morphology and function: delayed maturation, increased biogenesis, or increased fusion.

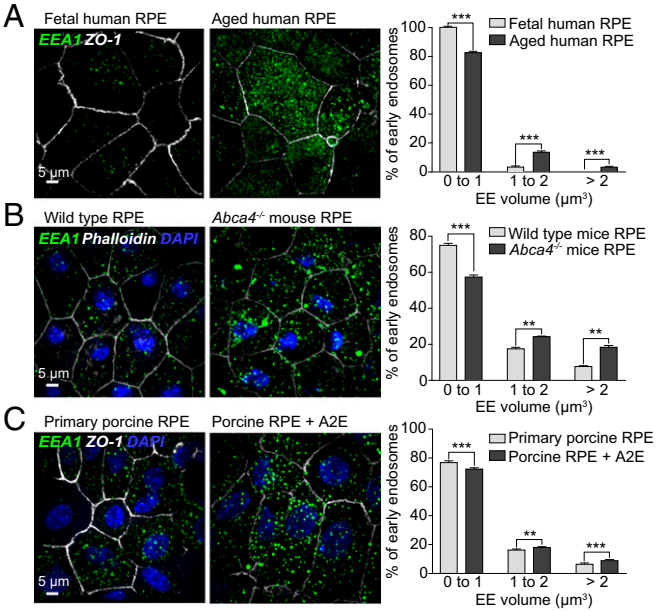

Fig. 1. Expansion of EEs in the RPE as a function of age and bisretinoid accumulation. (*A*) Immunostaining for EEA1 (green) and frequency histogram of EE volumes in fetal and aged human RPE. The tight junction protein ZO-1 (white) demarcates cell boundaries. Mean ± SEM, $n > 83$ cells per condition. ***$P < 0.001$, *t* test. (*B*) EEA1 immunostaining (green) and frequency histogram of EE volumes in RPE flatmounts from 6-mo-old wild-type and *Abca4*$^{-/-}$ mice. Phalloidin (white) demarcates cell boundaries; nuclei are stained with DAPI (blue). Mean ± SEM, $n = 3$ animals per group. **$P < 0.01$; ***$P < 0.001$, *t* test. (*C*) EEA1 immunostaining (green) and frequency histogram of EE volumes in polarized primary porcine RPE treated or not with the bisretinoid A2E. ZO-1 (white) and DAPI (blue). Mean ± SEM, $n >192$ cells per condition. **$P < 0.01$; ***$P < 0.001$, *t* test.

We reasoned that if enlarged EEs in the RPE are a result of a block in maturation, this should interfere with lysosomal degradation of phagocytosed OS discs, a critical function of the RPE. In mammals, rod OS disk shedding and phagocytosis are regulated by the circadian rhythm, with the peak occurring at light onset (14). Compared with wild-type mice, analyses of *Abca4*$^{-/-}$ RPE showed no difference in the numbers of LAMP1-labeled lysosomes (Fig. 3*A*), or kinetics of rhodopsin clearance at specific times after light onset (Fig. 3*B*). In polarized primary RPE monolayers fed porcine rod OS, there was no difference in the number of LAMP2-labeled lysosomes (Fig. 3*C*), trafficking of OS-containing phagosomes to lysosomes (Fig. 3*D*), or clearance of rhodopsin (Fig. 3*E*) in cells with A2E, compared with untreated cells. These data suggest that the subpopulation of enlarged EEs in RPE with bisretinoids does not have a discernible impact on endosome maturation or lysosomal degradation.

Apical Enrichment of Ceramide Stimulates EE Biogenesis and Fusion in the RPE. Analysis of EE volumes as a function of axial position within the cell revealed that the majority of enlarged EEs in *Abca4*$^{-/-}$ RPE and in primary RPE with A2E were located near the apical membrane (Fig. 4 *A* and *B*). Major membrane donors for EE biogenesis are endocytic vesicles that form by invagination and inward budding of the plasma membrane (1). A key modulator of membrane dynamics is ceramide, a cone-shaped lipid that promotes membrane invagination, budding, and fusion by forming nonlamellar phases with increased negative spontaneous curvature (15, 16). Based on our previous finding that RPE with bisretinoids accumulate ceramide due to cholesterol-mediated activation of ASMase (8), we hypothesized that increased ceramide at the RPE apical domain could drive the biogenesis of enlarged EEs. Consistent

Downloaded at Palestinian Territory, occupied on November 26, 2021

www.manaraa.com

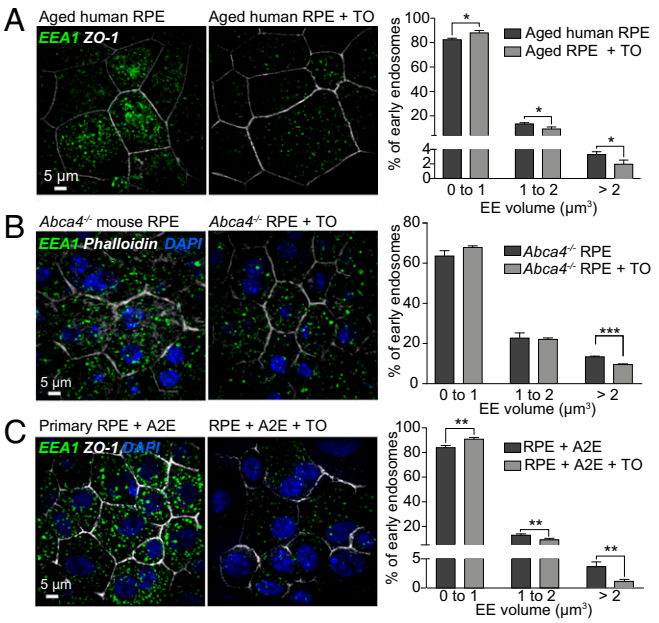

Fig. 2. Cholesterol removal corrects EE defects in RPE with bisretinoids. (*A*) EEA1-labeled EEs (green) and frequency histogram of EE volumes in aged human RPE treated with vehicle or 1 μM TO901317 (TO) for 16 h. Mean ± SEM, n >102 cells per condition. *P < 0.05, t test. (*B*) EEA1 immunostaining (green) and frequency histogram of EE volumes in RPE flatmounts from 6-mo-old *Abca4*$^{-/-}$ mice administered vehicle or TO for 4 wk. Mean ± SEM, n = 3 animals per group. ***P < 0.001, t test. (*C*) EEA1 immunostaining (green) and frequency histogram of EE volumes in polarized primary porcine RPE exposed to A2E and treated with vehicle or TO as in *A*. Mean ± SEM, n > 135 cells per condition. **P < 0.01, t test.

with this, immunostaining of RPE flatmounts revealed that ceramide is enriched near the apical surface in *Abca4*$^{-/-}$ mice RPE (Fig. 4*C*) and in primary RPE with A2E (Fig. 4*D*).

To further test our hypothesis, we performed live-cell imaging of primary RPE expressing CellLight Early Endosomes-RFP (RFP-Rab5) to examine EE biogenesis and membrane dynamics. To follow EE formation, we labeled the plasma membrane with CellMask, which allowed identification of "newborn" EEs that reside near the plasma membrane and retain the dye. We observed a significant increase in the number and volume of newborn Rab5^{+} EEs in RPE with A2E compared with control RPE (Fig. 4 *E* and *F* and Movies S1 and S2). Live imaging and analysis of EE membrane dynamics revealed a significantly increased rate of homotypic EE fusion in RPE with A2E relative to control RPE (Fig. 4 *G* and *H* and Movies S3 and S4). To confirm the role of ceramide in increased EE biogenesis and fusion in RPE with bisretinoids, we treated cells with desipramine. We have previously reported that desipramine reduces RPE ceramide by inhibiting ASMase (8). Here, as shown in Fig. 4 *G* and *H* and Movie S5, desipramine decreased fusion events and restored EE volumes. Taken together, our data support the hypothesis that excess ceramide in RPE with lipofuscin bisretinoids induces the expansion of EEs. How do these enlarged EEs impact the health of the RPE?

Enlarged EEs Enable Complement C3 Entry into the RPE. Recent studies suggest that EEs internalize the complement protein C3 from the extracellular milieu, resulting in C3 cleavage and activation within the cell (17–19). The complement cascade, which regulates the immune response and inflammation, can be triggered by multiple mechanisms, all of which converge at the point of C3 activation (10). Abnormal complement activity is strongly associated with AMD, and we and others have demonstrated increased complement-mediated inflammation in mouse models of Stargardt disease (9, 20, 21). In the retina, the RPE and other cell types, such as microglia, constitute a local source of C3 (22, 23). Low levels of C3 help maintain immune surveillance and visual function, whereas abnormal C3 activity has been implicated in AMD pathogenesis (22–25). We therefore asked if apical enlarged EEs participate in C3 internalization into the RPE. Analysis of RPE flatmounts from wild-type and *Abca4*$^{-/-}$ mice showed that *Abca4*$^{-/-}$ RPE had more C3 within enlarged EEs (Fig. 5*A*). Administration of desipramine to *Abca4*$^{-/-}$ mice by intraperitoneal injections for 4 wk significantly decreased EE volumes and C3 internalization (Fig. 5*A*), in agreement with our live-imaging data that desipramine decreases EE budding and fusion. Based on a recent report that cells specifically internalize the hydrolytic product of C3 [C3(H_2O)] but not native C3 (18), we performed live imaging of the uptake of fluorescently labeled purified human C3 [which is converted to C3(H_2O) after labeling (18)] in primary RPE cultures expressing RFP-Rab5. Cells with A2E internalized more C3 within enlarged EEs compared with

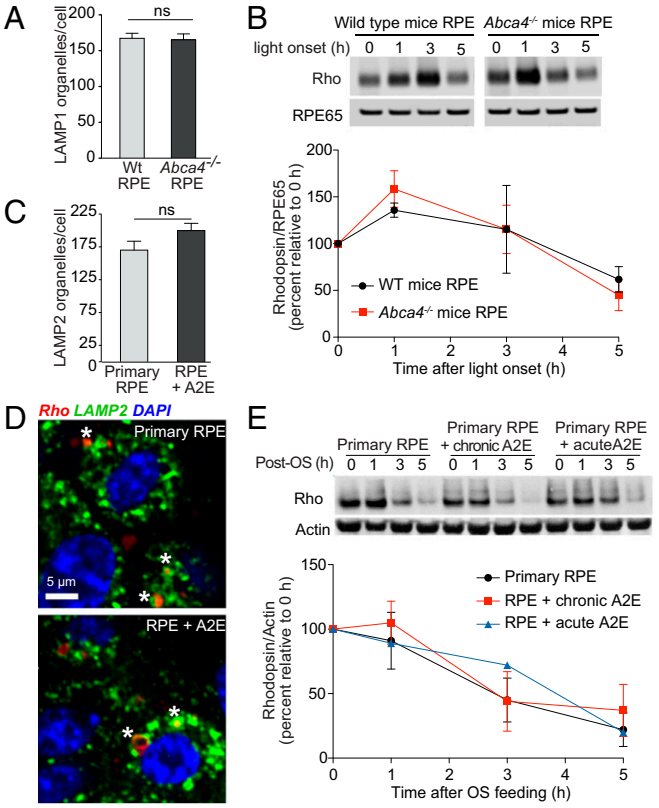

Fig. 3. Enlarged EEs do not impact clearance of phagocytosed photoreceptor OS. (*A*) Quantification of LAMP1^{+} lysosomes in wild-type and *Abca4*$^{-/-}$ mice. Mean ± SEM, n = 4 animals per condition; ns, not significant. (*B*) Rhodopsin degradation as a measure of phagocytosed photoreceptor OS clearance in 6-mo-old wild-type and *Abca4*$^{-/-}$ mice. RPE lysates were analyzed at specific times after light onset (0 h is 6:00 AM) by immunoblotting for rhodopsin. RPE65 was used as loading control. Graph shows percent of rhodopsin/RPE65 relative to values at light onset; n = 3 animals for each time point. (*C*) Quantification of LAMP2^{+} lysosomes in control and A2E-treated polarized primary porcine RPE. Mean ± SEM, $n \geq 300$ cells; ns, not significant. (*D*) Primary porcine RPE fed porcine OS were fixed and immunostained for rhodopsin (Rho; red) and LAMP2 (green). Nuclei were stained with DAPI (blue). Asterisks mark OS sequestered in lysosomes. (*E*) Rhodopsin degradation in primary porcine RPE cultures treated with A2E either chronically (50 nM for 3 wk) or acutely (10 μM for 6 h, with a 48-h chase). Cells were fed 40 OS per cell for 30 min, chased in fresh media for the indicated periods and analyzed by immunoblotting for rhodopsin. Actin was used as loading control. Graph shows percent of rhodopsin/actin relative to t = 0 from three independent experiments. Mean ± SEM, n = 3.

Downloaded at Palestinian Territory, occupied on November 26, 2021
www.manaraa.com

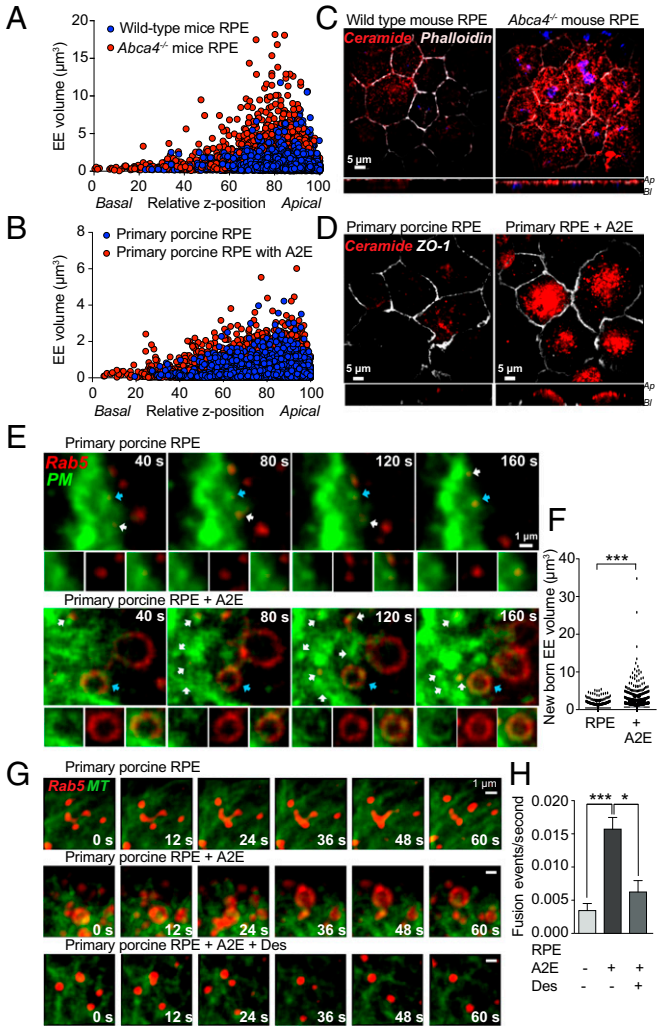

Fig. 4. Ceramide induces apical EE biogenesis and fusion in the RPE. (*A*) Distribution of EEs in wild-type (blue) and *Abca4*$^{-/-}$ (red) mouse RPE flat-mounts in each 0.2-μm confocal plane, from the bottom of the monolayer (*z*-position 0) to the top (*z*-position 100). Each circle represents an individual EE; pooled data from three animals per genotype. (*B*) Distribution of EEs in primary polarized porcine RPE monolayers ± A2E from >135 cells per condition. (*C*) *En face* and *xz* images of ceramide staining (red) in RPE flat-mounts of 6-mo-old wild-type and *Abca4*$^{-/-}$ mice. *Ap*, Apical; *Bl*, Basal. (*D*) *En face* and *xz* images of ceramide staining (red) in primary polarized porcine RPE monolayers ± A2E. *Ap*, Apical; *Bl*, Basal. (*E*) Stills (eightfold magnified) from live imaging of EE biogenesis in primary porcine RPE transduced with RFP-Rab5 (red) (Movies S1 and S2). The plasma membrane was labeled with CellMask (green). Arrows follow EE budding over time; *Insets* show a single EE (indicated by blue arrows) in separate and merged channels. (*F*) Volume of newborn EEs, ***$P < 0.001$, *t* test, $n = 41$ cells per condition. (*G*) Stills from live imaging of EE fusion in primary porcine RPE transduced with RFP-Rab5 (red) and tubulin-GFP (green). (*H*) Quantification of fusion events in *F*, *$P <$ 0.05, ***$P < 0.001$, *t* test, mean ± SEM, $n > 11$ cells per condition.

control cells, and desipramine treatment prevented this increase in C3 uptake (*SI Appendix*, Fig. S3*A*). Uptake of other endocytic cargo that travel through EEs, such as transferrin, is not affected in RPE loaded with A2E (*SI Appendix*, Fig. S3*B*), suggesting that C3 is specifically internalized into swollen EEs in RPE with bisretinoids.

Generation of Intracellular C3a Activates mTOR in the RPE. The majority (~80%) of internalized C3(H_2O) is recycled back to the extracellular space, whereas the remaining ~20% is processed by intracellular proteases (18). Proteolytic cleavage of C3 can generate biologically active (e.g., C3a) and inactive (e.g., iC3) fragments. Recent studies report that C3a is a key player in an intracellular complement system that regulates mTOR activity, metabolic reprogramming, and inflammation (10, 26). To establish that enlarged EEs facilitate C3a generation in vivo, we analyzed RPE cell lysates by immunoblotting and identified C3 cleavage products, including C3α′, C3β, C3a, and iC3b. Notably, C3a was detectable only in RPE lysates from *Abca4*$^{-/-}$ mice (Fig. 5*B*).

Next, to investigate whether intracellular C3a activates mTOR, we exposed primary RPE monolayers without or with A2E to fluorescently-labeled human C3 (C3-647) as in *SI Appendix*, Fig. S3*A*. We observed colocalization of C3-647 fluorescence signal with immunostaining for C3a, and a significant increase in phosphorylated mTOR [on S2448, indicative of active mTOR (27)] only in RPE with A2E (Fig. 5*C*). In T cells, cathepsin L (CTSL) has been identified as the protease that cleaves C3 to generate C3a. We were neither able to confirm expression of CTSL in the RPE, nor did we see an effect of a CTSL inhibitor (19) on C3a levels. This is not surprising because C3-activating proteases are likely to be cell-type specific (19). Desipramine treatment decreased C3a generation (Fig. 5*D* and *SI Appendix*, Fig. S3*C*) and mTOR phosphorylation (Fig. 5*E*) in RPE of *Abca4*$^{-/-}$ mice, providing further evidence that preventing EE expansion helps limit intracellular C3 activation.

Discussion

EEs are central to cell health because they regulate mechanisms involved in signaling, growth, and defense. Here, we show that in addition to their well-appreciated roles as sorting hubs, EEs in the RPE act as pathogenic hubs, where major triggers implicated in macular degenerations (bisretinoid and cholesterol accumulation, complement activation) converge to modulate downstream disease-associated pathways. Using multiple models including RPE from aged human donors and *Abca4*$^{-/-}$ mice, we identify ceramide-induced membrane remodeling as a mechanism that underlies the formation of enlarged EEs in RPE with bisretinoids. These studies have implications beyond the retina: ceramide is increased in AD patient brains (28), raising the intriguing possibility of synergism between ceramide and the recently described Rab5 hyperactivation mechanism (29) to promote EE enlargement in neurons. While mechanisms that underlie increased ceramide in AD are yet to be elucidated, impaired cholesterol metabolism is a key feature of the disease. This raises the possibility that the mechanism we identified in RPE with lipofuscin bisretinoids—cholesterol-mediated activation of ASMase (8)—could also play a role in increasing ceramide in the AD brain. In support of this, deleting ASMase improves neuronal health and cognition in a mouse model of AD (30, 31).

Our data demonstrate that in Stargardt disease mice, swollen EEs act as vehicles for C3 uptake into RPE with bisretinoids. Exciting recent studies on immune cells from the Kemper and Atkinson laboratories suggest that C3a generated by C3 proteolysis acts as an "intracellular stress detection system" that helps the cell adapt to changing environmental conditions (10, 26). C3 is among the oldest and most abundant of complement proteins, and a primitive form of C3 has been identified in sponges (32), which are multicellular organisms that lack tissues and organs. Thus, it is plausible that intracellular homeostatic functions of C3 preceded its well-known functions in the plasma (10, 26). In CD4$^+$ T cells, C3a activates the C3a receptor (C3aR) on lysosomes, resulting in low-level mTOR activation required for cell survival (19). C3a binding to C3aR on the cell surface leads to sustained mTOR activity, which modulates multiple stress pathways, including glycolysis and oxidative phosphorylation, cytokine secretion, and inflammasome activation (26).

Although these studies largely focused on immune cells, intracellular C3 stores have been identified in cells of nonimmune origin, such as epithelial cells, endothelial cells, and fibroblasts (19). Mechanisms involved in C3 activation in these cells and the

Downloaded at Palestinian Territory, occupied on November 26, 2021
www.manaraa.com

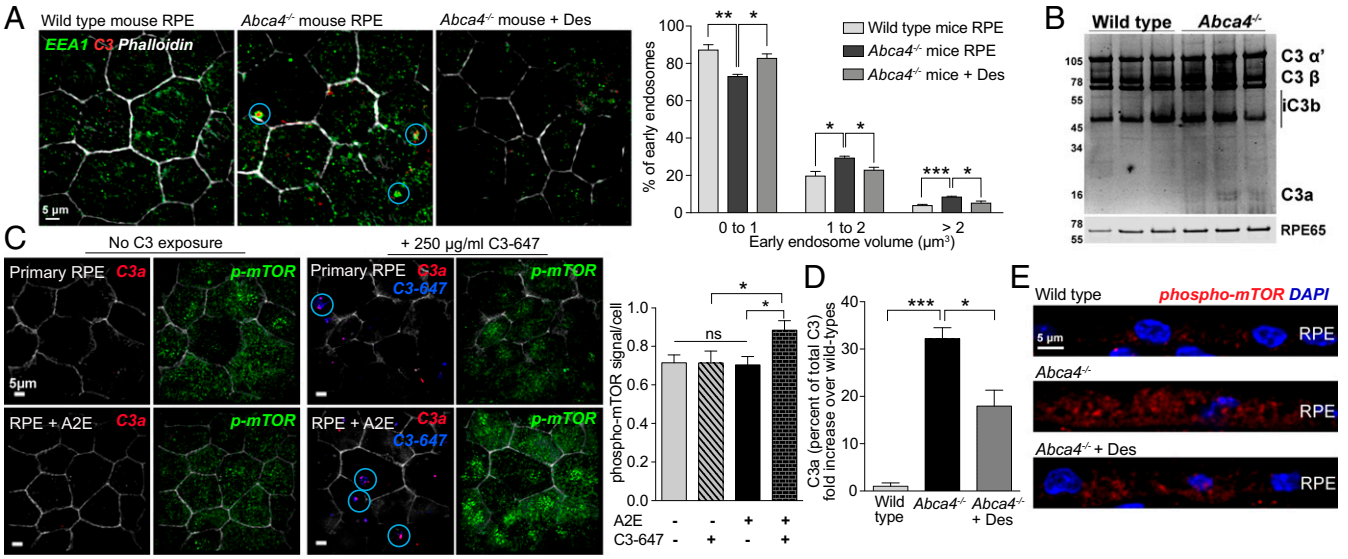

Fig. 5. Enlarged EEs facilitate C3a generation and mTOR activation in the RPE. (*A*) Single-plane *en face* images of EEA1 (green) and C3 (red) immunofluorescence and frequency histograms of EE volumes in RPE flatmounts in 6-mo-old wild-type and vehicle- or desipramine-treated *Abca4*$^{-/-}$ mice. Blue circles highlight enlarged EEs containing C3. **P* < 0.05; ***P* < 0.01; and ****P* < 0.001, multiple *t* test; *n* = 3 animals per group. (*B*) Representative C3 immunoblot of RPE lysates from 6-mo-old wild-type and *Abca4*$^{-/-}$ mice showing various cleavage products including C3a. RPE65 was used as a loading control. (*C*) Immunostaining for C3a (red) and phosphorylated mTOR [p-mTOR (S2448), green] in primary RPE monolayers exposed or not to C3-647 (blue). Graph shows quantification of phospho-mTOR signal. Mean ± SEM, **P* < 0.05 by one-way ANOVA with Bonferroni's multiple comparison test; ns, not significant. (*D*) C3a quantification in immunoblots of RPE lysates from wild type and *Abca4*$^{-/-}$ mice administered either vehicle or desipramine. Mean ± SEM, *n* ≥ 7 animals per group. **P* < 0.05 and ****P* < 0.001 by one-way ANOVA with Bonferroni's multiple comparison test. (*E*) Immunostaining for phosphorylated mTOR (red) in retinal cryosections from 6-mo-old wild-type and vehicle- or desipramine-treated *Abca4*$^{-/-}$ mice.

functional consequences are not yet clear. Here, we observed that increased C3a in RPE with bisretinoids is associated with chronic mTOR activation; however, whether C3a directly activates mTOR in the RPE remains to be established. Studies from our laboratory and others provide clues as to how this might impact RPE and retinal health: first, mTOR inhibition is required to initiate autophagy, and chronic mTOR activity in *Abca4*$^{-/-}$ RPE could explain the decreased autophagosome biogenesis that we previously reported in this model (8); second, sustained mTOR activation by chemical or genetic approaches in mice induces RPE dedifferentiation and hypertrophy (33); third, mTOR-mediated metabolic reprogramming increases RPE glycolytic flux, and the resulting decline in glucose delivery to the retina could contribute to photoreceptor degeneration (33); and fourth, inflammasome activation could promote RPE injury in geographic atrophy. Whether these sequelae occur directly in response to intracellular C3 are open questions.

The multiple levels of cross-talk between the complement, metabolic, and inflammatory pathways mediated by C3 make it a powerful regulator of cell homeostasis. Either deletion or overexpression of C3 causes retinal degeneration (25, 34), indicating that levels of C3 and its cleavage fragments must be carefully controlled in the retina. This could also explain why inhibitors of C3 and its activation have been unsuccessful in recent clinical trials for AMD (35). Normalizing C3 activity, rather than completely blocking it, might be a better therapeutic strategy for macular degenerations. In support of this approach, we demonstrate that the Food and Drug Administration-approved drug desipramine decreases ceramide, corrects endosomal defects, and limits C3a formation in Stargardt disease RPE. Pertinently, epidemiological studies indicate that the use of tricyclic antidepressants, like desipramine, is associated with a statistically significant protective effect against developing early AMD (36). In conclusion, the data presented here link bisretinoid-induced ceramide accumulation with abnormal endosome biogenesis and intracellular complement activation in the RPE, and provide a strong rationale for therapeutic targeting of ceramide in macular degenerations.

Materials and Methods

Mice and Drug Treatments. Wild-type (Jackson Laboratory 129S1/SvImJ) and *Abca4*$^{-/-}$ mice (Jackson Laboratory Abca4tm1Ght/J), both on Rpe65 Leu450 background, were raised under 12-h cyclic light with standard diet. Unless otherwise stated, mice were killed ∼4–6 h after light onset, eyes removed, and eyecups processed for immunohistochemistry or immunoblotting (11). All studies were approved by the University of Wisconsin–Madison animal care and use authorities. Five-month-old *Abca4*$^{-/-}$ mice (males and females) were intraperitoneally injected three times a week for 4 wk with either 100 µL of 10% DMSO (Sigma-Aldrich) in 1× phosphate buffer saline (PBS) or 20 mg/kg T0901317 (Cayman Chemicals) in 10% DMSO diluted in 1× PBS. For desipramine studies, mice were intraperitoneally injected three times a week for 4 wk with either 100 µL sterile, distilled water or 10 mg/kg of desipramine hydrochloride (Enzo Life Sciences) dissolved in sterile, distilled water.

Primary Porcine RPE Culture. To generate polarized monolayers, RPE isolated from porcine retinas were plated at confluence (∼300,000 cells/cm^2) onto collagen-coated Transwell filters (Corning), as described previously (8, 11).

Human RPE Cell Culture. RPE were isolated from human globes from donors aged between 67 and 93 y (The Eye-Bank for Sight Restoration, Inc., and Miracles in Sight), as described previously (37, 38). Human fetal RPE cultures were obtained from Lonza and grown in RtEBM media with growth supplements (all from Lonza) according to the manufacturer's instructions.

Treatments. Primary RPE cultures were treated with A2E (acute: 10 µM for 6 h and 48 h chase; chronic: 50 nM for 3 wk) to match levels found in the RPE of patients with Stargardt disease and in *Abca4*$^{-/-}$ mice (8). The LXR agonist T0901317 (Cayman Chemicals) was used at 1 µM for 16 h and the ASMase inhibitor desipramine hydrochloride (Enzo Life Sciences) was used at 10 µM for 3 h (8, 13).

Immunofluorescence and Immunohistochemistry. Depending on the experiment, polarized RPE monolayers and mouse RPE flatmounts were fixed and stained with primary antibodies to EEA1 (goat anti-EEA1 from Santa Cruz or rabbit anti-EEA1 from Abcam), C3 (MP Cappel), ceramide (Enzo Life Sciences), LAMP1 (Sigma-Aldrich), LAMP2 (Serotec), rhodopsin (Millipore), ZO-1 [mouse anti–ZO-1 (Invitrogen) for human RPE and rat anti–ZO-1 for porcine RPE], followed by AlexaFluor secondary antibodies, and sealed under coverslips

Downloaded at Palestinian Territory, occupied on November 26, 2021
www.manaraa.com

using VectaShield as a mounting medium. Retinal cryosections were stained with phospho-mTOR (Ser2448) antibody (Cell Signaling Technology) and processed as above. Slides were imaged with the Andor Revolution XD spinning disk confocal microscope with identical exposures and gains (8) using the 100× 1.49 NA objective.

Organelle Numbers, Volumes, and Position. EEA1- or LAMP1-labeled organelles were subjected to surface reconstruction using the Surfaces module, with the same intensity threshold applied to all images within a set of experiments (Imaris; Bitplane). The *z*-positions of EEs were plotted as percentage of cell height where the highest *z*-position was assigned as 100% and the bottommost as 0%.

Live Imaging of EE Dynamics. To follow EE biogenesis, primary porcine RPE expressing BacMam RFP-Rab5 were labeled with CellMask Deep Red (both from ThermoFisher) to delineate the plasma membrane and imaged immediately on a spinning disk confocal microscope (Andor). To follow EE fusion, cells expressing BacMam RFP-Rab5 and tubulin-GFP were imaged live. Analyses of EE formation, volumes, fusion, and fission events were performed on Imaris.

C3 Internalization and mTOR Activation. For live imaging, primary RPE cultures expressing BacMam RFP-Rab5 were incubated with 100 μg/mL AlexaFluor 647-labeled C3 (CompTech) for 15 min at 37 °C (18). Uninternalized C3-647 was removed and cells were imaged immediately. For mTOR activation experiments, polarized RPE on Transwell filters were incubated with 250 μg/mL AlexaFluor 647-labeled C3 for 30 min at 37 °C. Cells were washed, fixed, and stained with antibodies to C3a/C3a des Arg (1:100; Abcam), phospho-mTOR (Ser2448) (1:50; Cell Signaling Technology), and ZO-1.

C3 Immunoblotting. RPE lysates were resolved in Novex 10–20% Tricine gels, transferred onto nitrocellulose membranes (Invitrogen) and probed with antibodies to C3 (1:500; MP Cappel) and RPE65 (1:1,000; Novus), followed by IRDye secondary antibodies and visualized by Odyssey (LI-COR).

Outer Segment Clearance. To follow OS clearance in vivo, mice were killed at indicated times after light onset and eyes were harvested. To follow OS degradation in primary RPE cultures, cells were fed 40 porcine OS per cell for 30 min, and unbound OS were removed and replaced with normal growth media until cells were harvested at specific times. RPE lysates were resolved by SDS/PAGE, transferred to nitrocellulose membranes and probed with antibodies to rhodopsin (1:750, clone 4D2; Millipore) and actin (1:500; Santa Cruz) followed by HRP-conjugated secondary antibodies. Blots were visualized by ECL (ThermoFisher) and quantified with Image Studio (LI-COR).

Statistics. Data were analyzed using either a two-tailed *t* test with Welch's correction for unequal variances or one-way ANOVA with the Bonferroni multiple-comparisons posttest (GraphPad Prism). Unless otherwise stated, data are presented as mean ± SEM of ≥three independent experiments, with at least three to four replicates per condition per experiment.

ACKNOWLEDGMENTS. This work was supported by NIH Grants R01EY023299 and P30EY016665, and grants from Research to Prevent Blindness, BrightFocus Foundation (M2015350), the Wisconsin Partnership Program New Investigator Program, the Reeves Foundation, Macular Society UK, the Retina Research Foundation Rebecca Meyer Brown Professorship, and gifts from the Schuette-Kraemer family, the Stevens family, and the Christenson estate for macular degeneration research.

1. Huotari J, Helenius A (2011) Endosome maturation. *EMBO J* 30:3481–3500.
2. Jane-wit D, et al. (2015) Complement membrane attack complexes activate noncanonical NF-κB by forming an Akt+ NIK+ signalosome on Rab5+ endosomes. *Proc Natl Acad Sci USA* 112:9686–9691.
3. Zeigerer A, et al. (2015) Regulation of liver metabolism by the endosomal GTPase Rab5. *Cell Rep* 11:884–892.
4. Small SA, Simoes-Spassov S, Mayeux R, Petsko GA (2017) Endosomal traffic jams represent a pathogenic hub and therapeutic target in Alzheimer's disease. *Trends Neurosci* 40:592–602.
5. Lakkaraju A (2012) Endo-lysosome function in the retinal pigment epithelium in health and disease. *Adv Exp Med Biol* 723:723–729.
6. Bowes Rickman C, Farsiu S, Toth CA, Klingeborn M (2013) Dry age-related macular degeneration: Mechanisms, therapeutic targets, and imaging. *Invest Ophthalmol Vis Sci* 54:ORSF68-80.
7. Sparrow JR (2016) Vitamin A-aldehyde adducts: AMD risk and targeted therapeutics. *Proc Natl Acad Sci USA* 113:4564–4569.
8. Toops KA, Tan LX, Jiang Z, Radu RA, Lakkaraju A (2015) Cholesterol-mediated activation of acid sphingomyelinase disrupts autophagy in the retinal pigment epithelium. *Mol Biol Cell* 26:1–14.
9. Tan LX, Toops KA, Lakkaraju A (2016) Protective responses to sublytic complement in the retinal pigment epithelium. *Proc Natl Acad Sci USA* 113:8789–8794.
10. Liszewski MK, Elvington M, Kulkarni HS, Atkinson JP (2017) Complement's hidden arsenal: New insights and novel functions inside the cell. *Mol Immunol* 84:2–9.
11. Toops KA, Tan LX, Lakkaraju A (2014) A detailed three-step protocol for live imaging of intracellular traffic in polarized primary porcine RPE monolayers. *Exp Eye Res* 124:74–85.
12. Guziewicz KE, et al. (2017) Bestrophinopathy: An RPE-photoreceptor interface disease. *Prog Retin Eye Res* 58:70–88.
13. Lakkaraju A, Finnemann SC, Rodriguez-Boulan E (2007) The lipofuscin fluorophore A2E perturbs cholesterol metabolism in retinal pigment epithelial cells. *Proc Natl Acad Sci USA* 104:11026–11031.
14. LaVail MM (1976) Rod outer segment disk shedding in rat retina: Relationship to cyclic lighting. *Science* 194:1071–1074.
15. Stancevic B, Kolesnick R (2010) Ceramide-rich platforms in transmembrane signaling. *FEBS Lett* 584:1728–1740.
16. Holopainen JM, Angelova MI, Kinnunen PK (2000) Vectorial budding of vesicles by asymmetrical enzymatic formation of ceramide in giant liposomes. *Biophys J* 78:830–838.
17. Meilinger M, et al. (1999) Metabolism of activated complement component C3 is mediated by the low density lipoprotein receptor-related protein/alpha(2)-macroglobulin receptor. *J Biol Chem* 274:38091–38096.
18. Elvington M, Liszewski MK, Bertram P, Kulkarni HS, Atkinson JP (2017) A C3(H20) recycling pathway is a component of the intracellular complement system. *J Clin Invest* 127:970–981.
19. Liszewski MK, et al. (2013) Intracellular complement activation sustains T cell homeostasis and mediates effector differentiation. *Immunity* 39:1143–1157.
20. Radu RA, et al. (2011) Complement system dysregulation and inflammation in the retinal pigment epithelium of a mouse model for Stargardt macular degeneration. *J Biol Chem* 286:18593–18601.
21. Charbel Issa P, Barnard AR, Herrmann P, Washington I, MacLaren RE (2015) Rescue of the Stargardt phenotype in Abca4 knockout mice through inhibition of vitamin A dimerization. *Proc Natl Acad Sci USA* 112:8415–8420.
22. Mullins RF, Russell SR, Anderson DH, Hageman GS (2000) Drusen associated with aging and age-related macular degeneration contain proteins common to extracellular deposits associated with atherosclerosis, elastosis, amyloidosis, and dense deposit disease. *FASEB J* 14:835–846.
23. Natoli R, et al. (2017) Retinal macrophages synthesize C3 and activate complement in AMD and in models of focal retinal degeneration. *Invest Ophthalmol Vis Sci* 58:2977–2990.
24. Clark SJ, Bishop PN (2018) The eye as a complement dysregulation hotspot. *Semin Immunopathol* 40:65–74.
25. Hoh Kam J, Lenassi E, Malik TH, Pickering MC, Jeffery G (2013) Complement component C3 plays a critical role in protecting the aging retina in a murine model of age-related macular degeneration. *Am J Pathol* 183:480–492.
26. Kolev M, Kemper C (2017) Keeping it all going-complement meets metabolism. *Front Immunol* 8:1.
27. Guertin DA, Sabatini DM (2007) Defining the role of mTOR in cancer. *Cancer Cell* 12:9–22.
28. Filippov V, et al. (2012) Increased ceramide in brains with Alzheimer's and other neurodegenerative diseases. *J Alzheimers Dis* 29:537–547.
29. Nixon RA (2017) Amyloid precursor protein and endosomal-lysosomal dysfunction in Alzheimer's disease: Inseparable partners in a multifactorial disease. *FASEB J* 31:2729–2743.
30. Dinkins MB, et al. (2016) Neutral sphingomyelinase-2 deficiency ameliorates Alzheimer's disease pathology and improves cognition in the 5XFAD mouse. *J Neurosci* 36:8653–8667.
31. Lee JK, et al. (2014) Acid sphingomyelinase modulates the autophagic process by controlling lysosomal biogenesis in Alzheimer's disease. *J Exp Med* 211:1551–1570.
32. Poole AZ, Kitchen SA, Weis VM (2016) The role of complement in cnidarian-dinoflagellate symbiosis and immune challenge in the sea anemone Aiptasia pallida. *Front Microbiol* 7:519.
33. Zhao C, et al. (2011) mTOR-mediated dedifferentiation of the retinal pigment epithelium initiates photoreceptor degeneration in mice. *J Clin Invest* 121:369–383.
34. Cashman SM, Desai A, Ramo K, Kumar-Singh R (2011) Expression of complement component 3 (C3) from an adenovirus leads to pathology in the murine retina. *Invest Ophthalmol Vis Sci* 52:3436–3445.
35. Dolgin E (2017) Age-related macular degeneration foils drugmakers. *Nat Biotechnol* 35:1000–1001.
36. Klein R, et al. (2001) Medication use and the 5-year incidence of early age-related maculopathy: The Beaver Dam Eye Study. *Arch Ophthalmol* 119:1354–1359.
37. Fernandes M, McArdle B, Schiff L, Blenkinsop TA (2018) Stem cell-derived retinal pigment epithelial layer model from adult human globes donated for corneal transplants. *Curr Protoc Stem Cell Biol* 45:e53.
38. Blenkinsop TA, Salero E, Stern JH, Temple S (2013) The culture and maintenance of functional retinal pigment epithelial monolayers from adult human eye. *Methods Mol Biol* 945:45–65.

Downloaded at Palestinian Territory, occupied on November 26, 2021

www.manaraa.com